

The All Sky Automated Survey. Variable Stars in the 0^{h} - 6^{h} Quarter of the Southern Hemisphere. *

by

G. Pojmański

Warsaw University Observatory, Al Ujazdowskie 4, 00-478 Warsaw, Poland
e-mail: gp@sirius.astrouw.edu.pl

ABSTRACT

This paper describes the first part of the photometric data from the $9^{\circ} \times 9^{\circ}$ ASAS cameras monitoring the whole southern hemisphere in V -band. Data acquisition and reduction pipeline is described and preliminary list of variable stars is presented. Over 1,300,000 stars brighter than $V=15$ on 40,000 frames were analyzed and 3126 were found to be variable (1046 eclipsing, 778 regular pulsating, 132 Mira and 1170 other, mostly SR, IR and LPV stars). Periodic light curves have been classified using the fully automated algorithm, which is described in detail. Basic photometric properties are presented in the tables and thumbnail light curves are printed for reference. All photometric data is available over the INTERNET at <http://www.astrouw.edu.pl/~gp/asas/asas.html> or <http://archive.princeton.edu/~asas>.

Key words: *Catalogs -Stars:variables-general-Surveys*

1 Introduction

The All Sky Automated Survey (Pojmański 1997, 1998, 2000) has finally achieved its important goal - photometric monitoring of the large part of the sky (Paczyński 1997). After installing two wide-field ($9^{\circ} \times 9^{\circ}$) cameras in October 2000 (Pojmański 2001) ASAS gained capability to measure brightness of the observable stars on the nightly basis.

The prototype ASAS system using small commercial CCD camera, 135 mm f/1.8 telephoto lens and I -band (Schott RG-9, 3mm) filter was used in the years 1997-2000 to monitor 0.7% of the sky to the limiting magnitude of $I \sim 13$. During 3 years of operation it has collected over 50×10^6 measurements of over 150.000 stars and detected almost 4000 variable stars.

The instrument, data acquisition and reduction pipeline, the ASAS Catalog and summary of the variability search were described by Pojmański (1997, 1998, 2000),

In summer 2000 we have installed upgraded ASAS-3 system in the dome of the 10" astrograph in the Las Campanas Observatory (operated by the Carnegie Institution of Washington). New hardware consisted of the three independent instruments each equipped with the automated parallactic mount, imaging optics with standard filter, $2\text{K} \times 2\text{K}$ (14 um pixels) CCD camera and dedicated computer.

Two wide-field systems are equipped with the Minolta 200/2.8 APO-G telephoto lenses giving superb sharpness (FWHM < 2 pixels) but also strong vignetting (40-50 % in the corners). Field of view is $8.8^{\circ} \times 8.8^{\circ}$. The two systems are equipped with standard I and V filters.

*Based on observations obtained at the Las Campanas Observatory of the Carnegie Institution of Washington.

Narrow field instrument is $D = 250$ mm, $F = 750$ mm Cassegrain system with three element, Wynne-type field corrector. It gives sharp images (FWHM < 2.2 pixels) in the field of 2° diameter. With 2048×2048 CCD field of view is $2.2^\circ \times 2.2^\circ$. This system has I filter in its optical path.

Three AP-10 (Apogee) commercial cameras were purchased for the project. High readout noise ($> 10e^-$) and 14 bit ADC were accepted as a trade-off for 5 sec readout time. Unfortunately two of three systems did not meet factory specifications (increased noise resulting in substantially reduced sensitivity, failed thermo-cooler) and had to be sent for repair after first months of operation. ASAS-3 was left with only wide-field V -band camera running.

2 Observations

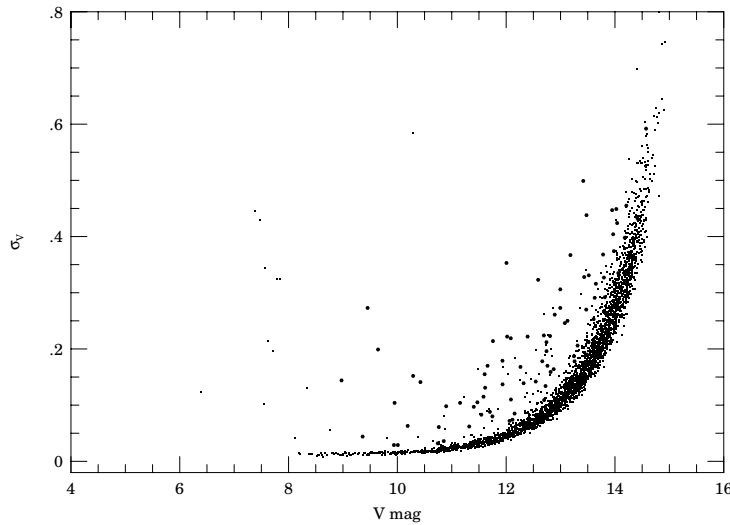


Fig. 1. Standard deviation σ_V vs. V -band magnitudes measured with the wide-field V camera and 3-minute exposures for the field centered on SMC. Larger dots denote detected variables. Small dots lying above 95 centile represent mostly "long-term" variables not recognized in this work.

Although mechanical quality of the mount allows for unguided exposures as long as 5-10 minutes for wide-field systems, only 3 minute exposures are taken in V -band giving the limiting magnitude of almost 15.0 and causing saturation of the stars brighter than $V = 8.5$.

The whole sky was divided into 709 $8^\circ \times 8^\circ$ fields of which 422 (60%) with $\delta < +20^\circ$ can be observed from Las Campanas (up to 300 on a single summer night). Due to the obscuration by the dome only fields with $\delta < +2^\circ$ were observed by the V instrument.

The routine observing schedule for each wide-field camera consists of cycling through the list of fields and picking up the one that is the most suitable for observation at the moment. Selection algorithm was not uniform enough, so equatorial fields were observed two times less often than the circumpolar ones.

Although the sky-flats are not best suited for the wide-field instruments we are using them both as the first order correction for vignetting and pixel-to-pixel sensitivity variation. Each night a series of sky-flat exposures is taken after the sunset, followed by the dark exposures.

Between 160 and 200 frames per night in V -band are taken each night (depending on the season), enabling camera to cover the whole available sky in less than two days. The raw data stream of one ASAS-3 instrument is about 1.5 GB per night. The loss-less

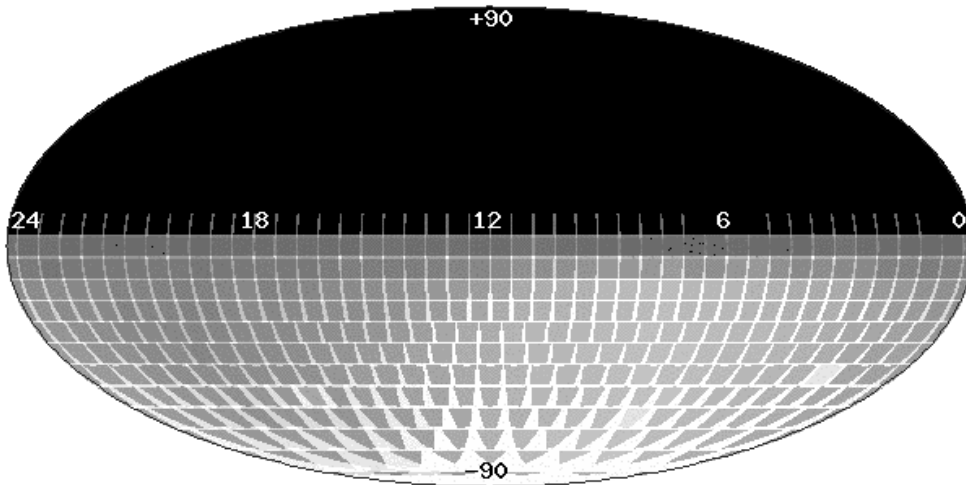


Fig. 2. Coverage of the sky with V -band observations after one year of ASAS-3 operation. White color corresponds to the area observed at least 250 times, dark gray - at least 30. Only fields centered within $0^{\text{h}} < \alpha < 6^{\text{h}}$ are analyzed in this paper.

compression reduces this stream to 0.7 GB per night (2-3 DAT-3 tapes per month), so we are considering some lossy compression in future.

3 Data Reduction

The data reduction pipe-line used for ASAS 1-2 observations was described by Pojmański (1998). ASAS-3 incorporates only some minor changes to that schematics.

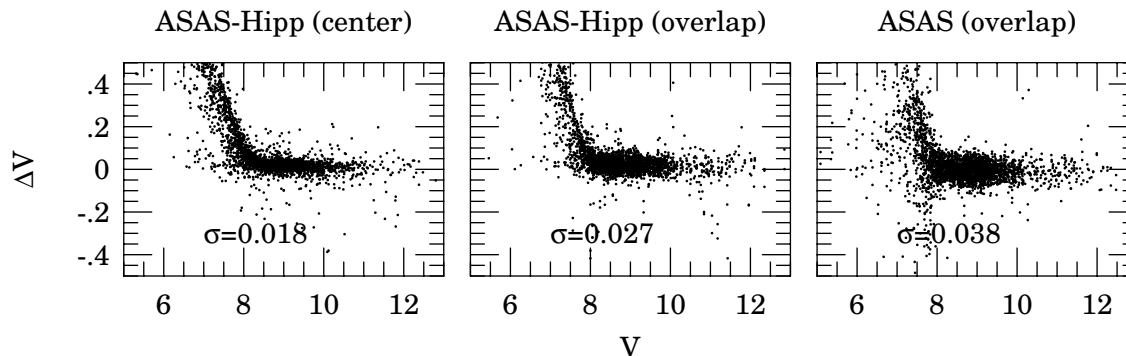


Fig. 3. Difference between Hipparcos and ASAS-3 magnitudes for all available stars.

Current optics gives sharp images and produces less scattered light than the previous one. In fact images can be so sharp (FWHM ~ 1.4 - 1.6 pixels) that only aperture photometry can properly deal with them. Therefore we are now making simultaneous photometry through five apertures varying in size from 2 to 6 pixels in diameter. Each aperture data is process separately, so one can use data obtained with the smallest one for the faint objects and with the largest one for the brightest objects in the catalog.

Reducing ASAS-2 data we partly managed to correct photometry for saturation and bleeding and have included overexposed stars in the ASAS Catalog. Unfortunately current CCD cameras do not allow for such correction and current photometry of the saturated images is practically useless.

Less scattered light in the optics (partly due to the smaller opening: $f/2.8$ vs. $f/1.8$) have substantially improved the quality of the sky-flats allowing us to obtain good first-order correction of the vignetting.

The astrometry is now based on the ACT catalog. Using 3-d order polynomials in X and Y we usually obtain positional accuracy better than 0.2 pixels (< 3 arcsec).

The zero-point offset of our photometry is based on the Hipparcos (Perryman *et al.* 1997) data. A few hundred Hipparcos stars are usually located in each 9×9 deg field. We use them for precise offset calibration. The rms scatter between ASAS and Hipparcos calculated for all stars lying close to the frame center is about 0.015 mag (Fig. 3a) Close to the edges it is significantly larger (Fig. 3b) due to systematic effects caused by non-perfect flat-fielding. Errors are most prominent (Fig. 3c) when we compare brightness of the stars located in the overlapping areas of the neighboring fields (Fig. 3c).

The final catalog is divided in two parts now. The first, flexible one is relatively slow, but is capable to store information about all sources detected on the frame. This catalog is regularly analyzed and significant measurements are moved into the second, fast-access part of the catalog. The remaining data (usually single entries caused by the image flaws) are archived separately.

All data processing is normally done in real time on the instrument's computer, but due to the necessity of fine-tuning of many elements of the pipe-line we are reprocessing the data from the tapes at the Warsaw head-quarters.

4 Variability Search

Data analyzed in this paper cover the period of one year (2001) of unattended operation. During that time all southern sky has been covered with observations at least 50-150 times. Over 50.000 frames have been collected in V-band. More than 10.000 for $0^h - 6^h$ quarter of the Southern Hemisphere alone. 1.3 million stars have been measured in this area more than 40 times. These stars were subject to variability analysis similar to that performed for the ASAS-2 data (Pojmański 2000).

First, light curves for each star in the field were extracted and median magnitude and dispersion were calculated (in each aperture separately). These were plotted on the magnitude-dispersion diagram (Fig. 1) and stars lying above the 95% centile were selected for the further analysis.

For each suspected star AOV period analysis (Schwarzenberg-Czerny 1989) was performed. Stars with statistics value larger than 10. were accepted. The other stars were subject to long-term variability tests: variance analysis in variable-length bins and trend analysis (average number of consecutive observations showing the same direction of brightness change). Proper thresholds for these observables were selected after tests. Finally all stars showing dispersion above 99.9% centile were added to the set.

As many as 18.000 stars have passed selection criteria and had to be further inspected. About 3.200 have passed visual inspection. The large number of rejected stars was due to several reasons: First - small number of observations, which usually forces AOV algorithm to produce spurious (or at least hard to verify) frequencies. Second - trends (slopes) in brightness changes of some stars which were partly produced by the increasing defocus of the optics in the course of the last two months. We decided not to include any light variation of this kind, although we are convinced some of these are real. Third - saturation, which has disappeared for some stars after they've got defocused.

The relative number of the variable stars detected so far (0.2% of the total) is 10 times lower than that obtained by ASAS 1-2 in the selected fields. This has been caused by several factors.

First, we have investigated only stars above 95% centile in the magnitude-dispersion diagram. while previously we have inspected almost 75% of the stars, discovering many low-amplitude variables. This will be done also for current data, but not earlier than more efficient algorithms for data selection are worked out.

Second, data span is one year now *vs.* almost three years previously. Since we have also omitted most of the slowly varying objects much lower number of long-term variables has been discovered. Previously we have discovered about 400 periodic stars (0.26%) and 3400 long-term ones (2.2%), while now about 2200 (0.16%) periodic and 1000 (0.08%) long-term.

Third, number of data points for each star is on average several times smaller than in ASAS-2 database.

Fourth, data sampling was different - a few times per night previously *vs.* once per night now. This resulted in significant aliasing. We will solve this problem in future observing each field for some time in the "high frequency" mode - at least several times per night. As for now we can only present our best choice and try to improve lists available on the INTERNET as soon as new data are available.

506 variable stars observed by ASAS-2 are located in the currently analyzed region. 466 of them were observed by the ASAS-3 system. Most of the others were faint in *I* band, so probably were too faint for the *V* instrument. One was bright (053820-6937.4 $I \sim 9.69$), but since it is irregular variable it might have faded below our *V* detection limit. Only about 100 of 466 stars were detected to be variable in *V*-band by the present analysis.

62 other objects were selected by the detection algorithm but were rejected after visual inspection. Only 3 of these were of "periodic" type and in all cases primary rejection reason was small number of points and low power in spectrum. For example ASAS 053936-7958.6 with an amplitude of 0.1 and only 40 data points was not found to be variable by the present analysis, while ASAS-2 has easily detected its variability with almost 4000 measurements.

Most of the other light curves that did not pass visual inspection were of the "long-term" type and were rejected because their slow variation or sparse data were not convincing enough.

The other 300 (65%) stars were not even preselected by the selection algorithm, again due to small number of data points or minute brightness changes. In most cases however, plotting their light-curves folded with the known period clearly reveals periodic variation.

5 Variability Classification

Only 2.000 of the 18.000 stars in the initial set of the candidate variable stars were selected by a quite robust long-term selection algorithm. Almost 1.500 of them have passed visual inspection.

The other 16.000 stars were selected by the AOV algorithm, thus their folded light curves had to be inspected visually one by one. Unfortunately, the relative number of true variables dramatically decreases as the AOV statistics comes closer to threshold, making verification process highly non-efficient.

Survey catalogs do not necessarily need to provide object classification, but their usefulness increases if they do. However, since volume of the data is growing rapidly, such step requires some automation providing necessary speed, repeatability and consistency.

Several attempts have been made so far to create classification machines based on neural networks and machine learning (e.g. Eyer and Blake 2002, Wozniak et al. 2002b)

or on direct parametric analysis (e.g. Udalski *et al.* 1999a, for cepheids, Ruciński 1993, 1997, Szymański, Kubiak, Udalski 2001 for contact binaries).

Here we propose simplified approach that mimics nonlinear neural network behavior. Its parameters ("weights") can be easily defined in terms of the light curve parameters. "Teaching" in this case is done by defining the multidimensional solids describing selected classes. Classification could then be done by selecting the closest solid in the multidimensional parametric space. To simplify our task we use carefully selected two-dimensional cross-section of that space.

Ruciński (1993, 1997) has shown that light curves of the contact configurations of W UMa systems can be easily described using only two coefficients, a_2 and a_4 , of the cosine series $\sum a_i \cos(2\pi i\theta)$. We have extended this approach tested behavior of the semi-detached and detached configurations in the a_2 - a_4 plane.

Several thousands theoretical light curves were calculated using the Wilson-Devinney (1971) code for a wide range of binary parameters: masses M_1, M_2 temperatures T_1, T_2 and radii R_1, R_2 characteristic for the main sequence O...M stars, periods P varying from the contact configuration to 100 days and inclinations i in the range of $60^\circ - 90^\circ$. For each combination of M_1, M_2 and P we have varied R_1 and R_2 between the main sequence and the Roche lobe sizes.

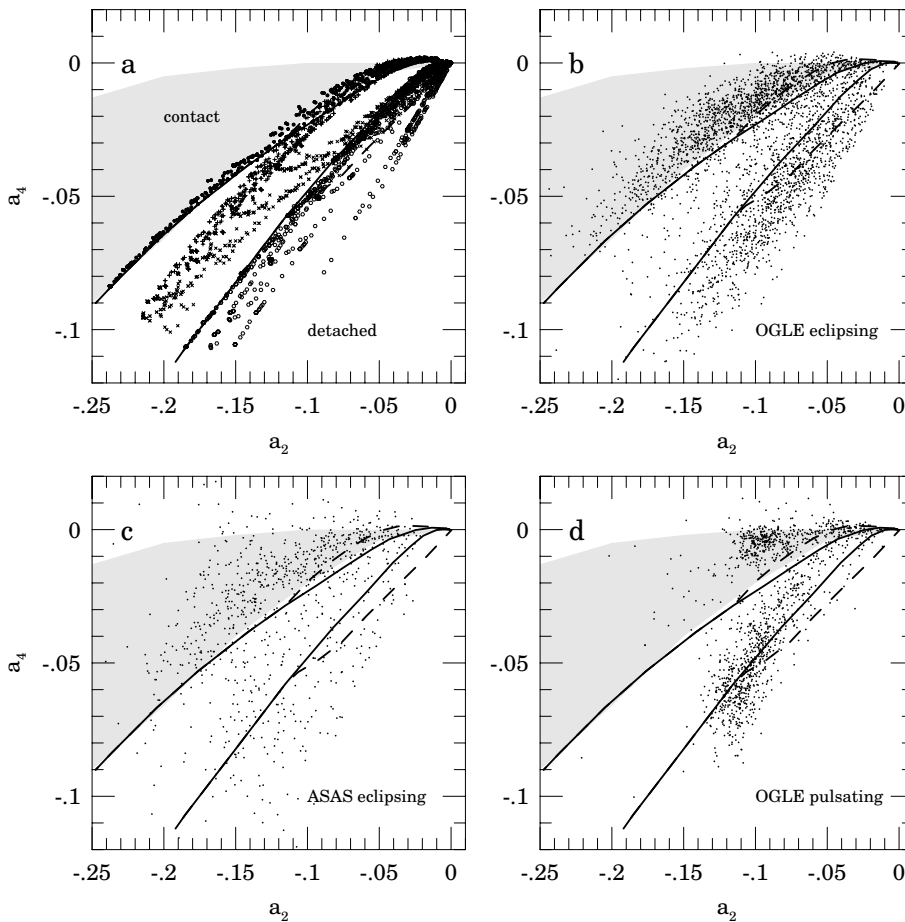


Fig. 4. Distribution of light curves in the $a_2 - a_4$ plane. a) Data obtained from the Wilson-Devinney simulation are plotted. Grey area encloses contact models calculated by Ruciński (1993). Two continuous lines delineate contact and detached configurations, while semi-detached systems are located between dashed lines. b) Eclipsing variables from the OGLE Bulge database (Wozniak 2002a). c) ASAS eclipsing binaries (this paper). d) OGLE Bulge pulsating variables.

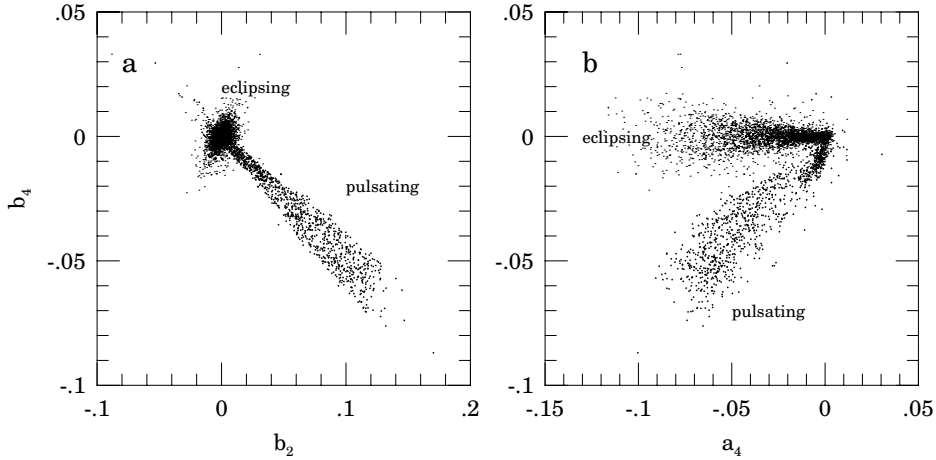


Fig. 5. Separation of eclipsing and pulsating variables in a) $b_2 - b_4$ and b) $a_4 - b_4$ planes. Data plotted are for the OGLE Bulge variables.

Harmonic series of the form:

$$\sum_{i=1}^4 (a_i \cos(2\pi i\varphi) + b_i \sin(2\pi i\varphi)) \quad (1)$$

was then fitted to all light curves.

Fig. 4a shows coefficients a_2 and a_4 . Filled and open dots represent contact and detached configurations respectively, while pluses and crosses denote semi-detached configurations with primary and secondary filling its Roche lobe, respectively. Grey area covers contact configurations calculated by Ruciński (1993, Fig. 6).

Fig. 4a clearly indicates that in most cases contact, semi-detached and detached configurations can be unambiguously distinguished in the $a_2 - a_4$ plane. However, looking at individual light curves one can note some confusion introduced by widely used EW , EB , EA classification of the light curves: contact or almost contact configurations do not necessarily have minima of the same depth; there are frequent semi-detached configurations with equal minima; detached binaries do not necessarily have flat maxima. Thus, although often used in such context, EW , EB and EA classes do not correspond entirely to the contact/detached discrimination. Since we feel that the later is physically more interesting, we would prefer to recognize “c”, “sd”, and “d” configurations. Thus we will classify as EC contact configurations lying above the upper line in Fig. 4a, as ED detached binaries located below the lower line, and as ESD remaining semi-detached systems located between the dashed lines.

In case of real data some additional steps have to be taken before applying Fourier decomposition. First the “base” frequency, f_0 , that equals to the frequency of the eclipsing system and is half of the pulsation frequency for the pulsating stars has to be located in the power spectrum. AOV spectrum puts most of the power either into $2f_0$, f_0 or even $2/3f_0$, depending on the light curve shape and distribution of observations - complicating automation of the process.

Fortunately a slightly slower ORTPER code (AOV Multiharmonic Periodogram for Uneven Sampling, Schwarzenberg-Czerny, 1996) usually properly selects $2f_0$ for the pulsating stars and f_0 or $2f_0$ for eclipsing light curves. The final test on f_0 is done performing Fourier decomposition using f_0 . In properly phased light curve we expect the a_2 term to be dominant, so if we obtain $a_4/a_2 > 1$. we have to halve the initial value of f_0 .

The second step necessary for direct comparison of the Fourier coefficients is consistent determination of the zero phase. We do that by locating minimum on the reconstructed light curve.

In the present work we use only the first 4 harmonics. This reduces our ability to recognize tiny features on the light curves in return for smaller coefficient scatter.

Large data set of uniform light curves is necessary to efficiently divide parametric volume into class solids. We have used 3 major sources of data: our own (ASAS) light curves that were provisionally classified into *DSCT*, *RRAB*, *RRC*, *DCEP*, *EW*, *EB* and *EA* classes; OGLE SMC and LMC cepheids (Udalski *et al.* 1999a, 1999b) carefully divided into *DCEP_{FU}* and *DCEP_{FO}* (fundamental and first overtone) classes; and subset of the OGLE Bulge variables (Wozniak 2002a), that were provisionally divided into pulsating and eclipsing groups.

In Fig. 4b the OGLE Bulge eclipsing variables (Wozniak 2002a) are plotted, while in Fig. 4c ASAS data from this paper. It is interesting that in case of OGLE data significant deficiency of the semi-detached systems could be spotted.

In Fig. 4d the OGLE Bulge pulsating stars are plotted to show that a_2 - a_4 plane cannot be used for separating pulsating and eclipsing systems. Instead b_2 - b_4 or a_4 - b_4 coefficient pairs (Fig. 5ab) provide necessary segregation.

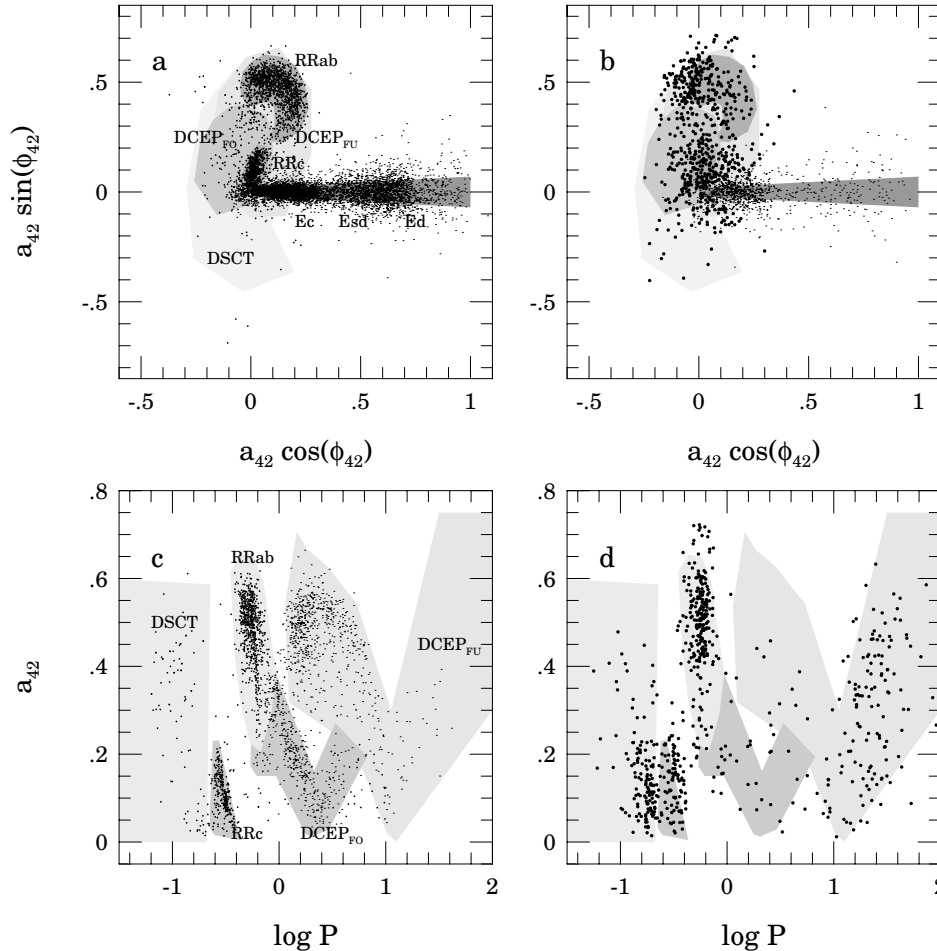


Fig. 6. Distribution of light curve parameters in the $a_{42} - \varphi_{42}$ and $\log P - a_{42}$ planes for OGLE (a,c) and ASAS (b,d) variables. Tiny dots in the upper panel are eclipsing binaries, while larger ones - pulsating.

Finally we need to recognize different types of pulsating stars. We have done this using $a_{42} = \frac{a_4}{a_2}$ vs. $\varphi_{42} = \varphi_4 - \varphi_2$ (radial coordinates, Fig. 6a,b) and $\log P$ vs. a_{42} (Fig.

6c,d) diagrams, on which categorized ASAS data and OGLE Bulge pulsating stars were plotted. The later one is an equivalent of the well known R_{21} vs. $\log P$ diagram used for cepheid classification. Although ASAS data were scattered, they provided necessary clues to define sharp polygons enclosing different classes of OGLE Bulge variables in both planes.

Besides the period P three other non-Fourier parameters describing light curves were needed to reduce the number of wrong classifications: two describing difference in minima and maxima levels and the third describing vertical asymmetry of the light curve (fraction of the measurements brighter than the average). They were necessary, because the fourth order harmonics could not properly recognize narrow, unequal minima or sharp maxima.

Process of automated classification is now straightforward: each class is described by a set of polygons in several cross-sections (planes) of the parametric space. In each plane score function is calculated: it equals 1.0 inside the polygon and decreases exponentially outside the polygon. The rate of decrease depends on the accuracy with which we determine the observable, so even large distances from the polygons could be accepted for noisy data. All scores are multiplied and the class with the highest result is selected as a winner. If other classes have similar scores (at least 75% of the maximum) multiple classification is accepted. If the highest score is below 0.50 uncertainty flag (:) is added, while for very low scores (less than 0.2) general class of *PULSE* is applied. So far we have defined three eclipsing classes: *EC*, *ESD*, *ED* and six pulsating: *DSCT*, *RRAB*, *RRC*, *DCEP_{FU}*, *DCEP_{FO}*, *M*.

Such algorithm has many advantages. It is fast, easy to verify and very flexible. Adding new observables (like location in color-magnitude or period-luminosity diagrams, spectral type etc.) is instant and needs only defining a new polygon in the parametric space. The obvious disadvantage is that only predefined classes could be selected.

In this paper, using only one color photometric data, we are in fact classifying data according to the the light curve shape and period only. Therefore caution must be taken not to over-interpret results: Many *RRC* objects might be in fact *EC* or *DSCT*. The algorithm will usually recognize and mark such situations. *DCEP* classes are based on SMC/LMC data and will not entirely correspond to Galactic objects. *DCEP_{FU}* are usually easily recognized by their *RRAB*-like shapes, but around $\log P = 1$. many sinusoidal cases are encountered and probability of wrong classification increases. *M* (Mira) class was defined for objects with $\Delta V > 2$. and $P > 70^d$, so some SR, IR and even CV objects might have been also classified as *M*.

We have discovered many “M” shaped variables, both in ASAS and OGLE data, with periods of tens of days. The algorithm tends to classify them as *EC* or *ESD*, implying they are contact or semi-detached giant stars. In fact in case of OGLE variables most of them are located close to the Red Clump (Udalski, 2002), so there is no inconsistency. That is why we did not restrict *EC* class to the short periods only.

Another problem with automated classification is caused by semiregular and irregular variables, which often show strong signal in the power spectrum. Unless detected by other means these stars have a good chance to be falsely classified. We have tried to define *SR* and *IR* classes in terms of long-term variations in the light curve, but results are not satisfactory yet. For the present analysis we decided to relay on the initial visual inspection of light curves, during which we have selected about 1100 irregular ones that were marked as *MISC* and were not subject to automated classification. These are mostly semiregular (*SR*), irregular (*IR*), slow irregular (*L*), *LBV* and other less regularly changing stars with time scales of variation between 10 and 200 days.

6 The catalog

Current list of candidate variable stars in the first quarter of the Southern Hemisphere contains 3126 stars.

For each star the following data are provided: ASAS identification ID (coded from the star's α_{2000} and δ_{2000} in the form: $hhmmss - ddm.m$), period P in days (or characteristic time scale of variation for irregular objects), T_0 - epoch of minimum brightness (for eclipsing stars) or maximum brightness (for pulsating stars), V_{max} - brightness at maximum, ΔV - amplitude of variation, $Type$ - one of the predefined classes: EC , ESD , ED , $DSCT$, RRC , $RRAB$, $DCEP_{FU}$, $DCEP_{FO}$, M , $PULS$ and $MISC$.

67 stars marked with ":" were inspected visually, and in about 20 cases original classification was changed (in most cases for highly distorted ED curves, that were classified as pulsating ones). 680 objects have multiple classification. For 330 cases this is exclusively due to EC/ESD or ED/ESD confusion, but for 180 other this is a more serious EC/RRC or $EC/DSCT$ double classification. Quite often visual inspection may help to remove such degeneracy.

ELL and SR suffixes were added in several (54 and 45) cases for almost purely sinusoidal light curves and for evident long term changes respectively.

Search for detected variables in the SIMBAD database revealed only 800 matches with stars known to be variable (almost 200 of them are in the the SMC and LMC fields), so over 75% of stars are probably new detections.

Table 1 contains a compact version of the catalog. Only four columns are listed for each star: identification ID , period P , V , and ΔV . Column ID also contains some flags - ":" if classification was uncertain, "?" if multiple classes were assigned, "v" if SIMBAD lists a star to be variable. Table 2 summarizes classification results.

Figs. 7 through 39 in the Appendix show thumbnail pictures of all light curves. Only ID is given for each. For periodic variables phase in the range (-0.1 - 2.1) is plotted along the x -axis, while for Mira's and miscellaneous stars - HJD in the range (2451800-2452300). On the y -axis magnitudes are given. Larger ticks always mark 1 magnitude intervals and vertical span is never smaller than 1 mag.

The full catalog of variable stars observed by the ASAS system containing more classification details and complete photometric data is available over the INTERNET:

<http://www.astro.uw.edu.pl/~gp/asas/asas.html>

or

<http://archive.pinceton.edu/~asas>

Table 1
Continued

ID	<i>P</i>	<i>V</i>	ΔV	ID	<i>P</i>	<i>V</i>	ΔV	ID	<i>P</i>	<i>V</i>	ΔV
<i>Stars classified as MISC.</i>											
060128-0354.1	27.96	10.85	0.20	060130-2527.9	90.9	12.49	1.17	060139-1558.1	55.7	9.98	0.46
060143-6931.5	61.4	11.43	0.52	060150-7035.6 v	193	10.03	1.36	060151-2106.3 v	424	10.12	0.61
060151-2127.7	64.4	11.41	0.36	060201-0422.0	48.5	9.19	0.21	060205-7040.5 v	31.21	8.52	0.16
060246-1943.7	73.5	10.02	0.64	060249-2100.1	21.84	12.22	0.20	060306-5754.7	57.7	11.17	0.44
060346-6942.6 v	122	8.95	0.45	060349-1217.8	67.3	10.59	0.25	060400-0357.8 v	54.5	10.87	0.35
060421-1709.7	45.9	11.90	0.22	060457-2212.5	108.7	12.60	0.86	060520-2505.6	128	9.81	0.49
060524-5729.6	127	10.76	0.34	060600-6040.7	33.96	9.73	0.25	060612-0830.3 v	85.2	10.92	0.31
060617-0705.9	336	12.54	1.93	060628-0927.3	31.21	10.30	0.17	060639-2706.1	48.7	9.91	0.19
060643-1245.5	121	12.47	0.85	060645-1239.0	127	11.24	0.74	060649-6044.6	121	11.75	0.87
060652-0812.0	51.1	10.86	0.36	060701-0254.9	26.13	9.35	0.78	060741-2052.4	63.9	8.86	0.19
060810-1406.8	49.0	10.87	0.24	060834-0042.8 v	87.3	11.19	0.53	060848-1302.4	150	12.67	0.30
060912-1428.8	58.1	12.92	0.65	060920-2104.6	38.9	10.73	0.27	060925-1306.1	45.2	11.01	0.30
060942-8541.4	59.6	11.95	0.34	060947-2228.8 v	168	10.41	0.65	060949-1143.7	84.7	9.94	0.39
060951-2231.8 v	47.3	9.53	0.48	061046-6024.0	62.8	10.90	0.64	061248-7736.7	52.8	11.55	1.67
061446-7659.7	27.22	11.28	0.23	062432-8343.0	62.8	10.69	0.58	064333-8555.8	316	13.61	0.93
064624-8538.4	320	11.18	0.24	064629-8450.5	203	12.92	1.31	064951-8243.6	184	10.37	0.62
065208-8517.8	146	11.56	0.37	074530-8449.7	300	12.68	1.76	075342-8727.4	128	11.14	0.56
080813-8556.6	54.1	10.88	0.36	091527-8714.5	77.4	13.37	0.80	092930-8721.6	60.2	11.09	0.50
094432-8713.6	39.2	10.11	0.19	095013-8725.3	15.13	10.69	0.12	100512-8615.0	48.4	11.98	0.37
102744-8617.9	48.2	11.03	0.26	110752-8632.4	157	12.87	0.87	111701-8835.6	51.8	11.57	0.34
112039-8704.1	166	11.70	0.31	114738-8622.9	110.1	12.66	1.07	120449-8723.1	127	11.54	0.40
122647-8702.0 ?	57.9	11.45	0.36	124002-8530.7	71.5	11.96	0.42	125351-8609.9	47.5	12.13	0.61
125353-8727.4 v	54.5	10.03	0.36	130015-8520.2	53.8	10.65	0.39	132030-8552.4 v	253	8.81	0.48
140041-8519.4	20.2	10.75	0.28	140634-8522.9	26.8	9.76	0.17	155630-8547.5 v	167	11.32	1.43
162726-8602.7	63.9	11.21	0.64	164538-8611.8	77.7	12.37	0.65	165107-8708.2 v	59.0	9.09	0.32
170225-8703.3	32.46	11.21	0.33	171030-8623.0	222	9.97	1.85	171931-8638.5 v	84.5	11.77	2.30
182927-8654.3	93.5	12.83	0.42	192802-8813.4	75.8	12.09	0.31	193325-8900.4	53.9	10.83	0.40
202901-8605.2	153	11.92	0.32	203912-8437.6	79.4	11.75	0.70	204429-8713.6	54.9	12.00	0.43
212153-8627.9	29.10	8.68	0.21	215503-8606.7	32.06	9.80	0.14	215650-8151.5	158	12.10	0.53
220020-8654.1	89.1	10.67	0.87	222132-8024.9	91.1	12.10	0.63	222201-8440.0 v	310	8.22	0.65
223301-8039.8	48.8	9.95	0.32	223908-8011.3	40.3	11.37	0.16	224737-7827.3	302	13.51	1.85
224759-7834.0	46.0	10.92	0.40	225242-8618.5	29.50	10.43	0.16	225636-8359.0	41.4	11.63	0.31
225937-7745.6	394	11.48	0.36	230409-7856.5	156	9.27	0.53	230856-8425.8	80.6	9.71	0.53
231138-8357.9	100.8	8.86	0.69	231447-7507.5	74.5	10.67	0.89	231708-8548.1	79.0	10.39	0.62
231818-8523.3	255	11.52	0.36	231908-8702.2	0.200480	11.04	0.14	232054-8434.2	28.40	9.40	0.19
232310-6212.3	42.3	11.21	0.33	232348-7128.0	77.6	10.62	0.55	232511-7606.3 v	40.8	8.33	0.26
232513-7703.0 v	263	11.85	2.00	232641-6901.0	130	11.03	0.80	232859-6002.0	166	12.86	0.74
232903-6446.0 v	79.7	9.30	0.59	232950-8213.9	86.1	12.89	0.76	233003-6821.1	55.8	11.30	0.44
233524-5503.1 v	39.8	10.78	0.56	233614-8331.0	86.6	12.13	0.69	233713-6044.2	45.8	9.44	0.22
233849-6923.0	56.2	11.61	0.35	233951-5549.9	50.8	11.94	0.50	234303-0730.2	61	8.77	0.24
234406-3405.2	61.1	10.83	0.64	234423-5829.6	38.5	10.03	0.21	234523-0208.8	47.7	10.11	0.38
234547-6257.7	42.4	10.83	0.22	234708-4548.9	78.9	10.93	1.12	234945-4317.1 v	57.6	10.01	0.29
235007-1417.8	84.7	10.16	0.49	235010-8651.1	68.7	11.19	0.63	235054-3517.8	159	12.07	0.60
235115-0245.8	127	12.22	1.14	235215-1551.3 v	139	8.26	1.89	235258-7752.9 v	48.2	11.01	0.28
235331-1000.3	16.14	9.04	0.17	235440-3046.1 v	46.8	9.98	0.24	235442-7700.5	106.9	11.71	0.49
235514-4459.8	49.1	11.96	0.49	235651-7928.1	46.2	10.15	0.40	235705-5213.3	50.0	10.10	0.37
235905-5634.6 v	244	7.14	1.77	235935-2952.0	218	10.52	0.11	235952-3452.2	67.1	11.75	0.24

Table 2

Number of various types of variable stars detected on
5000 sq. deg by ASAS-3 *V* camera.

Type	Count	Type	Count
<i>DCEP_{FU}</i>	192	<i>EC</i>	655
<i>DCEP_{FO}</i>	69	<i>ESD</i>	250
<i>DSCT</i>	148	<i>ED</i>	141
<i>RRAB</i>	247	<i>M</i>	132
<i>RRC</i>	113	<i>MISC</i>	1170
<i>PULS</i>	9		

7 Conclusions

We have presented preliminary results of the search for variable stars in the southern hemisphere. Only a quarter of available data covering right ascension between 0^h - 6^h has been presented in this paper. Over 3000 variable stars were found so far among 1,300,000

stars brighter than $V \sim 15$ mag. Comparison to the ASAS-2 data suggests, that number of variable stars should increase 3-10 times, as more observations are collected.

Most of these stars belong to the "periodic" class, as we have not included many candidate objects with the "long-term" variation. There is a large subset of bright ($V < 12$ mag) detached binaries - useful for distance scale calibration - perfect targets for small size spectroscopic instruments.

Fully automated classification algorithm that we have described in this paper, efficiently separates stars into predefined classes. For a good quality data its efficiency reaches 100% in those regions of the parametric space, where the classes do not overlap. For poor data or overlapping regions alternative classes are always proposed. Currently our algorithm works properly only if the highest peak in the power spectrum corresponds to the true frequency or one of its harmonics, which is not necessary true for noisy, poorly sampled data. What is still missing is a robust algorithm that will allow to separate light curves into strictly periodic and irregular ones.

However, at this time we feel it is better to publish imperfect data and to allow a broad range of astronomers to see the diversity of raw results and to work on variety of scientific topics. Note a recent paper by Pietrukowicz (2001), who used the past ASAS data to determine period changes in cepheids in the LMC.

Processing of the remaining ASAS data is in progress, so we plan to release next parts of this catalog soon. Also, four ASAS instruments are taking data, covering the whole southern sky each night. Over 120,000 images have been collected so far in V , I and R bands, covering the whole hemisphere more than 300 times. Soon real time photometry will be achieved, finally allowing us to setup the Early Warning System.

8 Acknowledgments

This project was made possible by a generous gift from Mr. William Golden to Dr. Bohdan Paczyński, and funds from Princeton University. It is a great pleasure to thank Dr. B. Paczyński for his initiative, interest, valuable discussions, and the funding of this project.

I am indebted to the OGLE collaboration for the use of facilities of the Warsaw telescope at LCO, for their permanent support and maintenance of the ASAS instrumentation, and to The Observatories of the Carnegie Institution of Washington for providing the excellent site for the observations. I am especially indebted to Marcin Kubiak for providing selected light curves from the OGLE Bulge database.

This research has made use of the SIMBAD database, operated at CDS, Strasbourg, France.

This work was partly supported by the KBN 2P03D01416 grant.

References

- Eyer, L. and Blake, C. 2002, *Radial and Nonradial Pulsations as Probes of Stellar Physics, ASP Conference Series*, **Vol. 259**, 160.
- Paczyński, B. 1997, "The Future of Massive Variability Searches", in *Proceedings of 12th IAP Colloquium: "Variable Stars and the Astrophysical Returns of Microlensing Searches"*, Paris (Ed. R. Ferlet), p. 357.
- Perryman, M.A.C. et al. 1997, *Astron. Astroph.*, **323**, L49.

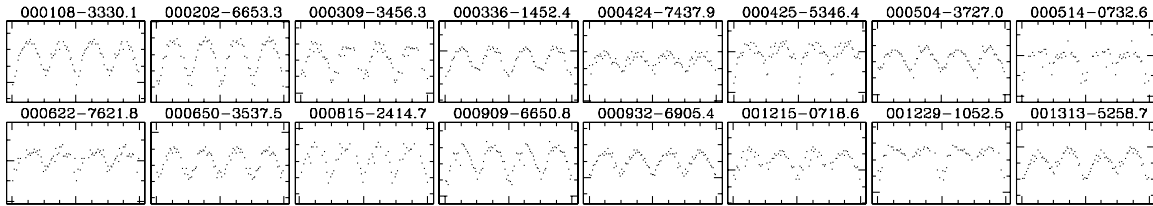
- Pojmański, G. 1997, *Acta Astr.*, **47**, 467.
- Pojmański, G. 1998, *Acta Astr.*, **48**, 35.
- Pojmański, G. 2000, *Acta Astr.*, **50**, 177.
- Pojmański, G. 2001, *in: Small Telescope Astronomy on Global Scales, ASP Conference Series Vol. 246, IAU Colloquium*, **183**, 53.
- Pietrukowicz, P. 2001, *Acta Astr.*, **51**, 247.
- Ruciński, S. 1993, *PASP*, **105**, 1433.
- Ruciński, S. 1997, *Astron. J.*, **113**, 1112.
- Schwarzenberg-Czerny, A. 1989, *MNRAS*, **241**, 153.
- Schwarzenberg-Czerny, A. 1996, *Astrophys. J.*, **460**, L107.
- Szymański, M., Kubiak, M., Udalski, A. 2001, *Acta Astr.*, **51**, 259.
- Udalski, A., Soszyński, I., Szymański, M., Kubiak, M., Pietrzyński, G., Wozniak, P., Żebruń, K. 1999a, *Acta Astr.*, **49**, 223.
- Udalski, A., Soszyński, I., Szymański, M., Kubiak, M., Pietrzyński, G., Wozniak, P., Żebruń, K. 1999b, *Acta Astr.*, **49**, 437.
- Udalski, A. 2002, *private communication.*, , .
- Wilson, R. E. and Devinney, E. J. 1971, *Astrophys. J.*, **166**, 605.
- Wozniak, P., Udalski, A., Szymański, M., Kubiak, M., Pietrzyński, G., Soszyński, I., Żebruń, K. 2002a, *Acta Astr.*, **52**, 129.
- Wozniak, P. *et al.* 2002b, *American Astronomical Society Meeting*, **199**, 130.04.

Appendix.

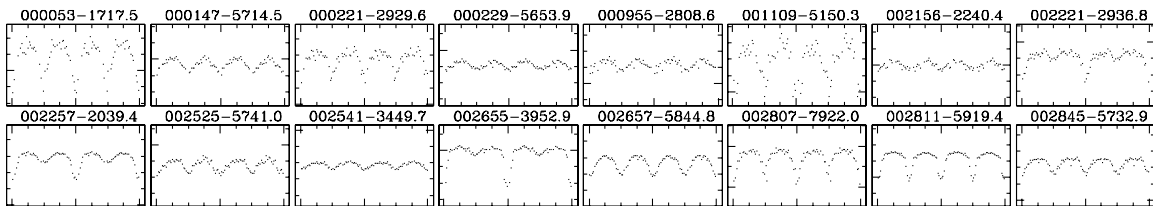
ASAS Atlas of Variable Stars. 0^h - 6^h Quarter of the Southern Hemisphere.
Only first 16 light curves of each type are presented here. Complete set of thumbnails can
be obtained from

<http://www.astrouw.edu.pl/~gp/asas/appendix.ps.gz> or

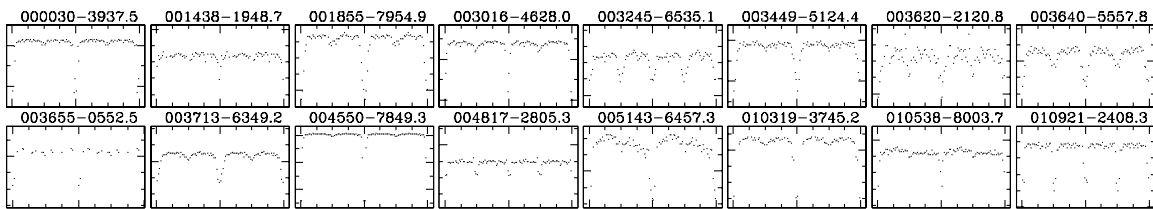
<http://archive.princeton.edu/~asas/appendix.ps.gz>



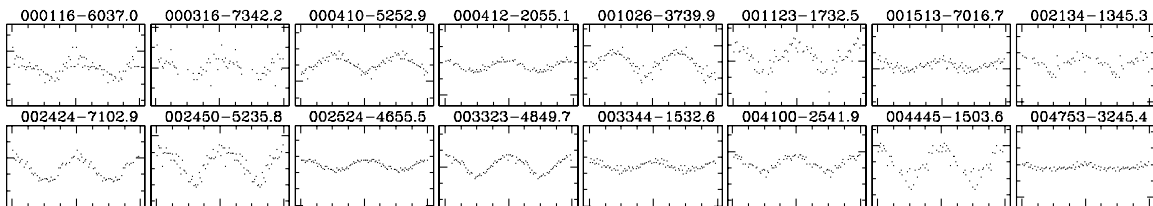
Stars classified as EC.



Stars classified as ESD.



Stars classified as ED.



Stars classified as DSCT.

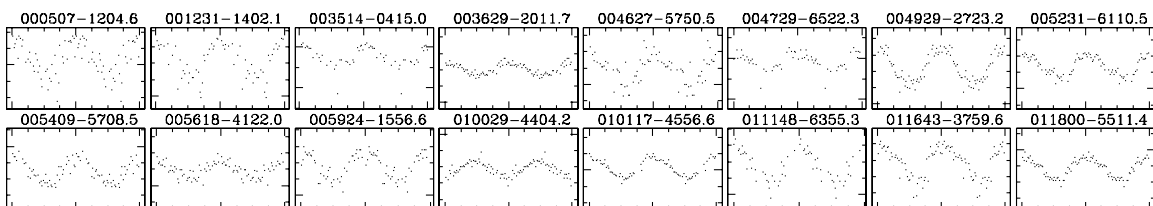
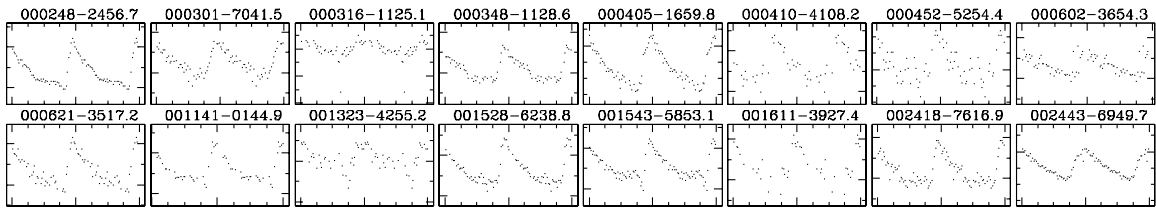
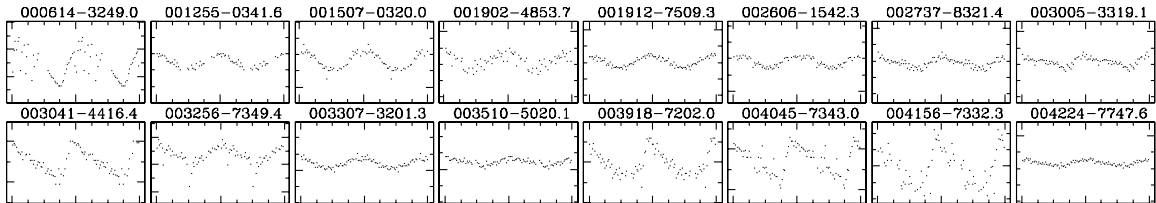


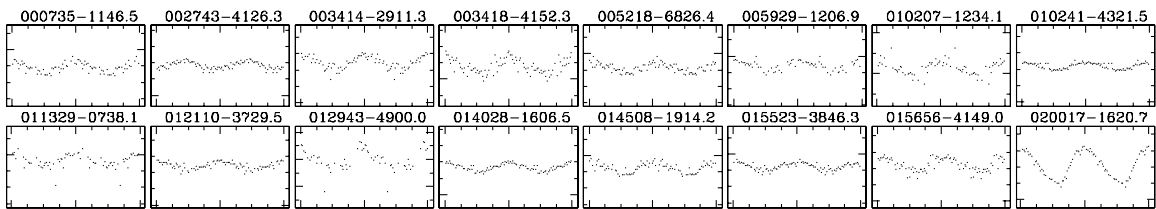
Fig. 7. Stars classified as RRC.



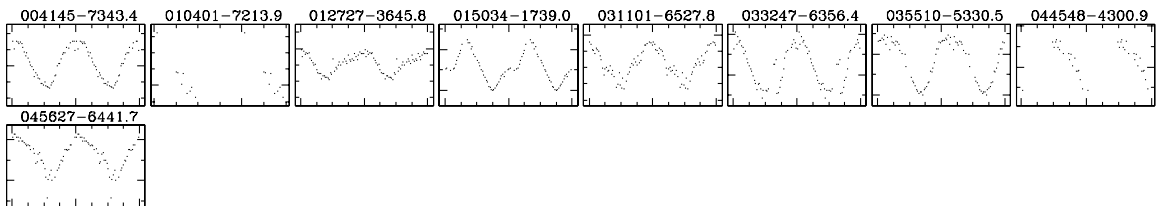
Stars classified as RRAB.



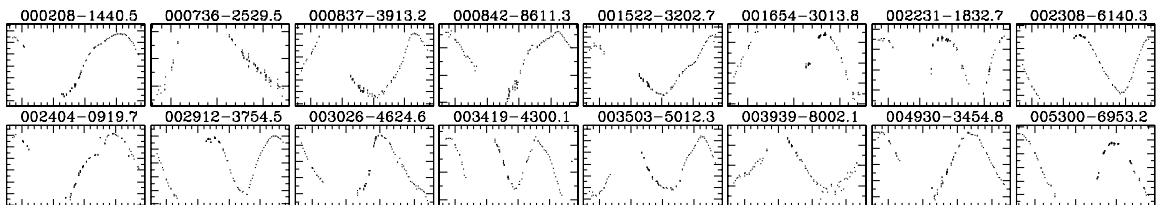
Stars classified as DCEP-FU.



Stars classified as DCEP-FO.



Stars classified as PULS.



Stars classified as MIRA.

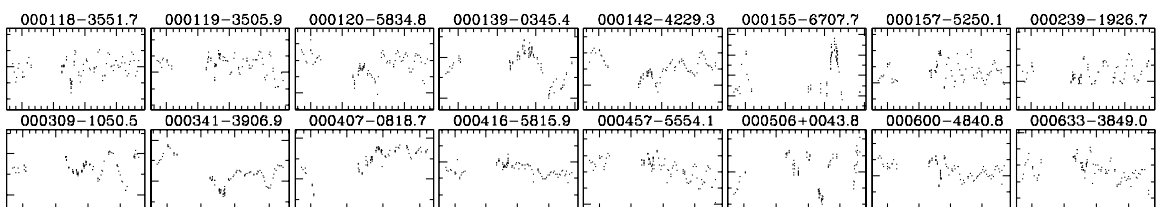


Fig. 8. Stars classified as MISC.